Water Research 240 (2023) 120084

Contents lists available at ScienceDirect

Water Research

journal homepage: www.elsevier.com/locate/watres

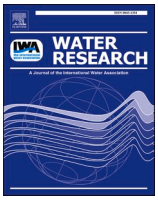

High-frequency sensor data capture short-term variability in Fe and Mn concentrations due to hypolimnetic oxygenation and seasonal dynamics in a drinking water reservoir

Nicholas W. Hammond [a], François Birgand [b], Cayelan C. Carey [c], Bethany Bookout [c], Adrienne Breef-Pilz [c], Madeline E. Schreiber [a,*]

[a] Department of Geosciences, Virginia Tech, United States
[b] Department of Biological and Agricultural Engineering, North Carolina State University, United States
[c] Department of Biological Sciences, Virginia Tech, United States

ARTICLE INFO

Keywords:
Hypolimnetic oxygenation
Iron
Manganese
Spatiotemporal resolution
Spectrophotometer
Sensors

ABSTRACT

The biogeochemical cycles of iron (Fe) and manganese (Mn) in lakes and reservoirs have predictable seasonal trends, largely governed by stratification dynamics and redox conditions in the hypolimnion. However, short-term (i.e., sub-weekly) trends in Fe and Mn cycling are less well-understood, as most monitoring efforts focus on longer-term (i.e., monthly to yearly) time scales. The potential for elevated Fe and Mn to degrade water quality and impact ecosystem functioning, coupled with increasing evidence for high spatiotemporal variability in other biogeochemical cycles, necessitates a closer evaluation of the short-term Fe and Mn dynamics in lakes and reservoirs. We adapted a UV-visible spectrophotometer coupled with a multiplexor pumping system and partial least squares regression (PLSR) modeling to generate high spatiotemporal resolution predictions of Fe and Mn concentrations in a drinking water reservoir (Falling Creek Reservoir, Vinton, VA, USA) equipped with a hypolimnetic oxygenation (HOx) system. We quantified hourly Fe and Mn concentrations during two transitional periods: reservoir turnover (Fall 2020) and HOx initiation (Summer 2021). Our sensor system successfully predicted mean Fe and Mn concentrations and trends, ground-truthed by grab sampling and laboratory analysis. During fall turnover, hypolimnetic Fe and Mn concentrations began to decrease more than two weeks before complete mixing of the reservoir, with rapid equalization of epilimnetic and hypolimnetic Fe and Mn concentrations in less than 48 h after full water column mixing. During the initiation of HOx in Summer 2021, Fe and Mn displayed distinctly different responses to oxygenation, as indicated by the rapid oxidation of soluble Fe but not soluble Mn. This study demonstrates that Fe and Mn concentrations are sensitive to changes in redox conditions induced by stratification and oxygenation, although their responses to these changes differ. We also show that high spatio-temporal resolution predictions of Fe and Mn can improve drinking water monitoring programs and reservoir management practices.

1. Introduction

Elevated levels of iron (Fe) and manganese (Mn) in lakes and reservoirs have negative consequences for ecosystem health and water quality. Increasing Fe concentrations have been linked to the long-term browning of lakes, which has numerous, significant ecological consequences (Kritzberg et al., 2020). Mn contamination of drinking water can pose risks to human health, especially to children (Wasserman et al., 2006). Furthermore, elevated concentrations of both metals negatively affect the taste, odor, and appearance of water and can damage water supply infrastructure through corrosion and deposition (World Health Organization 2017). As a result, the U.S. Environmental Protection Agency (USEPA) has established secondary standards for Fe and Mn concentrations in drinking water of 0.3 and 0.05 mg/L, respectively (USEPA 2021).

As Fe and Mn are redox-sensitive elements, their abundance in aquatic systems is largely influenced by dissolved oxygen (DO) concentrations (Hem 1972; Davison 1993). The oxidation state of Fe and Mn

* Corresponding author.
E-mail address: mschreib@vt.edu (M.E. Schreiber).

https://doi.org/10.1016/j.watres.2023.120084
Received 21 November 2022; Received in revised form 11 May 2023; Accepted 14 May 2023
Available online 18 May 2023

in natural waters is dominated by two forms: insoluble, oxidized Fe(III) and Mn(IV), and soluble, reduced Fe(II) and Mn(II) (Davison 1993). In most aquatic systems under circumneutral pH, this oxidation state is determined by the redox conditions at a given point in space and time. Under oxic conditions, Fe and Mn are generally present as insoluble Fe (III) and Mn(IV) solids in rocks and sediments. However, thermal stratification in lakes and reservoirs can create anoxic conditions in the hypolimnion and bottom sediments, promoting the microbial reduction of Fe and Mn in sediments and the subsequent release of soluble, reduced Fe and Mn into the water column (Lovely 1991). In such settings, soluble Fe and Mn can accumulate in hypolimnetic waters throughout the stratified period (McMahon 1969; Davison 1993).

An increasingly used in situ approach for mitigating water quality issues in drinking water reservoirs is hypolimnetic oxygenation (HOx), which creates oxic conditions in previously anoxic waters and creates a thicker aerobic zone in bottom sediments (e.g., Beutel and Horne 1999; Dent et al., 2014; Gerling et al., 2014). For the case of metals, by increasing oxygen availability in the hypolimnion, HOx operation hinders the release of soluble Fe and Mn into sediment pore waters, slows upward diffusion into the water column, and promotes Fe and Mn oxidation and precipitation in the hypolimnion (Preece et al., 2019). HOx systems have been shown to effectively reduce soluble Fe and Mn in the hypolimnion of drinking water reservoirs (Gantzer et al., 2009). However, removing soluble Mn from the water column requires more sustained oxygen inputs, due to its slower oxidation reaction kinetics (Bryant et al., 2011; Munger et al., 2016). To optimize water treatment using HOx systems, it is essential for drinking water managers to understand both the short-term (sub-weekly) and long-term (monthly to yearly) Fe and Mn dynamics in supply reservoirs.

Although Fe and Mn cycling in temperate lakes and reservoirs has predictable seasonal trends dictated by thermal stratification, there is a lack of research on short-term Fe and Mn dynamics. Quantifying short-term trends requires high-frequency data, which we define as having a temporal resolution of daily or shorter. To our knowledge, there is no standard definition for classifying data as 'high-frequency' or trends as 'short-term.' Thus, we developed operational definitions based on the contrast with traditional monitoring frequencies, which are typically weekly or longer (e.g., Marcé et al., 2016). The paucity of previous research on Fe and Mn cycling at sub-weekly scales represents a key knowledge gap, given that biogeochemical process rates can fluctuate rapidly over hourly to daily time scales (McClain et al., 2003). Studies have identified diel signals in the cycles of numerous biogeochemical variables, including Fe and Mn, and many biological and chemical processes in aquatic environments operate on hourly to daily scales, often with significant impacts on nutrient cycling and ecosystem productivity (Istvánovics et al., 2004; Nimick et al., 2011; Kurz et al., 2013). Additionally, episodic hydrologic events, which may be missed by traditional sampling methods, can have pronounced effects on biogeochemical cycling dynamics (e.g., Marcé et al., 2016, Coraggio et al., 2022).

Studies analyzing the efficacy of HOx systems have observed substantial changes in Fe and Mn concentrations in response to changes in oxygenation (Dent et al., 2014; Munger et al., 2019). For example, Dent et al. (2014) found that total Fe and Mn concentrations decreased by 71% and 73%, respectively, after 8 h of oxygenation of a previously-anoxic reservoir hypolimnion. Munger et al. (2019) found that Fe and Mn sediment fluxes into the water column were 1.4 and 4.5 times higher, respectively, two weeks after the onset of hypolimnetic anoxia in a reservoir. The dynamic behavior of Fe and Mn concentrations in response to both management and natural processes (e.g., seasonal thermal stratification) underscores the importance of quantifying these complex dynamics, which could have substantial implications for drinking water management and water quality monitoring. To date, monitoring programs have been hindered by the coarse temporal frequency of months to seasons necessitated by traditional manual sampling and laboratory analysis techniques.

Recent developments in sensor technology have enabled high-frequency collection of some water quality variables in situ, without the need for manual sampling and laboratory analysis (Porter et al., 2009; Rode et al., 2016; Kruse 2018). However, most high-frequency sensors are only capable of measuring a single variable at a time and typically have a low spatial resolution. Moreover, numerous water quality variables, including Fe and Mn, lack instrumentation capable of unattended, reagent-less, high-frequency measurement.

To circumvent the limitations of current sensor technology, spectrophotometers have been designed to measure water quality variables in situ at a high frequency using multi-wavelength absorbance patterns in the ultraviolet-visible (UV–vis) spectrum. These sensors do not require chemical reagents and are capable of measuring multiple variables simultaneously. To date, UV–vis spectrophotometers have been successfully used to measure chemical variables that have a strong correlation with known peaks in their absorbance spectra, such as nitrate, dissolved organic carbon, and total suspended solids (Etheridge et al., 2014; Sakamoto et al., 2009). Additionally, several studies have had success using them to measure concentrations of other biogeochemical variables without well-defined spectral peaks, such as Fe, total phosphorus, soluble reactive phosphorus, and dissolved silica (Birgand et al., 2016; Etheridge et al., 2014; Vaughan et al., 2018). Although Fe and Mn are not known to have well-defined spectral peaks, they absorb and scatter light at wavelengths across the UV–vis spectrum and they can affect the absorbance of a water sample through complexation with organic molecules (Poulin et al., 2014; Weishaar et al., 2003; Xiao et al., 2013). Therefore, the covariance between the variable of interest (e.g., Fe or Mn) and the overall "color matrix" of the water (the combination of multiple light-sensitive proxies) can be detected in the UV–vis absorbance spectra and used to predict concentrations of the variable of interest with statistical algorithms (Birgand et al., 2016). Laboratory-measured concentrations from manually collected samples are then subsequently used to develop predictive models that correlate known concentrations with absorbance spectra.

Numerous algorithms exist for calibrating UV–vis absorbance spectra to observed concentrations, but the most commonly-employed method is partial least squares regression (PLSR) (DiFoggio 2000; Birgand et al., 2016; Vaughan et al., 2018). PLSR is well-suited for modeling relationships within data that have a large number of highly correlated explanatory variables and relatively few observations, such as multi-wavelength spectral measurements (Wold et al., 2001). Previous studies have used in situ spectrophotometers coupled with PLSR models to predict water quality variables in a variety of environments, including streams, lakes, estuaries, and oceans (Sakamoto et al., 2009; Avagyan et al., 2014; Etheridge et al., 2014; Birgand et al., 2016; Vaughan et al., 2018). However, to the best of our knowledge, only one study (Birgand et al., 2016) has evaluated the potential of this method to observe the high-frequency dynamics of metals in stratified reservoirs.

In their study, Birgand et al. (2016) designed a multiplexor sequential sampling system to pump water from different depths in a reservoir to one spectrophotometer. This combined pumping system was developed because a single spectrophotometer cannot capture the rapid changes in elemental concentrations that occur along the strong thermal gradients with depth in lakes and reservoirs. Additionally, the cost of in situ spectrophotometers ($8000–25,000 USD as of 2023) prohibits the acquisition of multiple units needed to characterize spatial (depth) dynamics. This system has proven to be able to characterize variable reservoir biogeochemical concentrations over both depth and time (Birgand et al., 2016).

In this study, we used the system developed by Birgand et al. (2016) - i.e., an in situ spectrophotometer coupled with a multiplexor pumping system - and PLSR modeling to predict high-frequency Fe and Mn concentrations at nine depths in a seasonally-stratified drinking water reservoir. We then used this approach to observe the short-term (sub--weekly) variability of Fe and Mn concentrations during two distinct transitional periods: reservoir turnover in Fall 2020 and initiation of

HOx operation in Summer 2021. The objectives of this study were to: 1) predict high-resolution Fe and Mn concentrations using spectral absorbance data coupled with PLSR modeling, 2) identify whether Fe and Mn concentrations exhibit temporal variability across spatial (depth) gradients, and 3) quantify the effects of reservoir turnover and hypolimnetic oxygenation on Fe and Mn concentrations. We provide a detailed overview of our method below for interested readers and show how it can be applied to provide high-frequency Fe and Mn data at multiple depths in our focal reservoir.

2. Methods

2.1. Study site

Field data were collected at Falling Creek Reservoir (FCR), a small (0.12 km^2, maximum depth = 9.3 m), dimictic reservoir located in Vinton, Virginia, USA (Fig. 1, Gerling et al., 2014). FCR was constructed in 1898 and is managed as a drinking water reservoir by the Western Virginia Water Authority (WVWA) in Roanoke, VA. The summer stratified period at FCR typically lasts from May to October. FCR is located in a forested catchment with one primary inflow and several smaller tributaries. Due to the underlying geology, which consists of Fe- and Mn-rich rocks of the Blue Ridge and Piedmont Provinces (Woodward, 1932), this region has elevated Fe and Mn concentrations in surface and groundwater (Chapman et al., 2013), motivating the need for water quality interventions (e.g., Bryant et al., 2011).

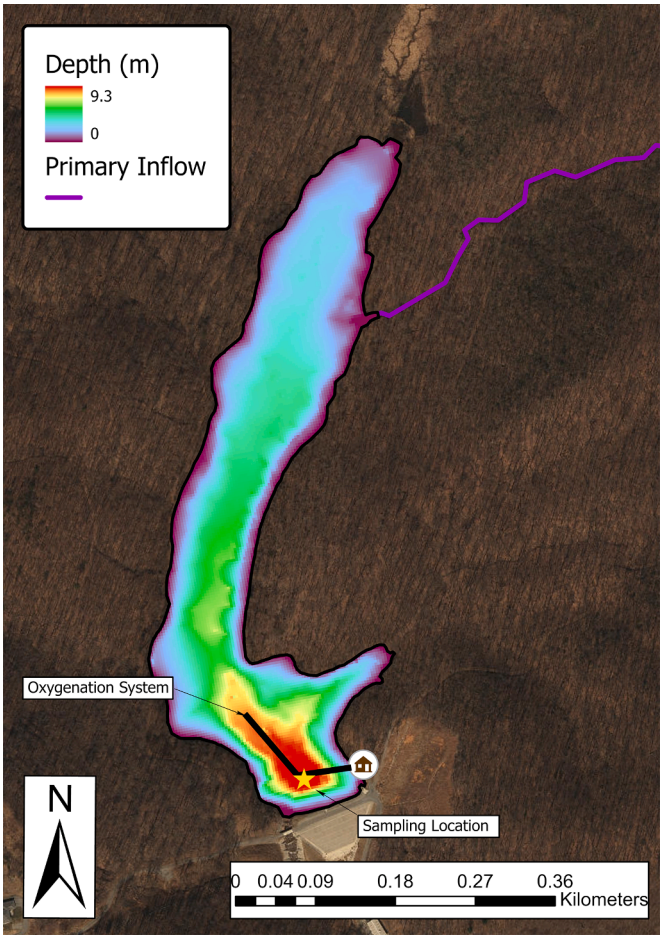

Fig. 1. Bathymetric map of Falling Creek Reservoir, Vinton, VA, USA (37.302913°N, −79.837070°W) depicting the primary sampling location (star icon) and hypolimnetic oxygenation (HOx) system. The HOx system consists of outlet piping with a distribution header (black line) and an oxygen contact chamber (shed icon).

FCR contains a HOx system, which can be activated and deactivated to control DO concentrations in the hypolimnion without altering thermal stratification or water temperature (Fig. 1, Gerling et al., 2014). The HOx system at FCR was activated from 29 June 2020 until 2 December 2020, when it was turned off for the winter period. It remained deactivated from 2 December 2020 until 11 June 2021, at which point it was turned back on and remained activated until the end of the study period on 21 June 2021. During its activation periods, the HOx added concentrated oxygen (~95% purity) at its maximum operation level (25 kg/d) to the hypolimnion (Gerling et al., 2014).

FCR is equipped with sensors that continuously monitor the physical, chemical, and meteorological conditions at the reservoir's deepest spot, which was the primary sampling location in this study (Fig. 1). DO sensor data was collected using a YSI EXO2 (Yellow Springs, OH) deployed at 1.6 m and two In-Situ RDO-PRO-X sensors (Fort Collins, CO) at 5 m and 9 m (Carey et al., 2022b). Ten-minute resolution temperature measurements were collected by in situ sensors deployed every meter from the surface to the reservoir sediments (Carey et al., 2022b). To quantify the intensity of reservoir thermal stratification during each deployment, we calculated Schmidt stability (J m^{-2}, Idso 1973) using temperature measurements and bathymetric data from FCR (Carey et al., 2022c) as inputs to the R package *rLakeAnalyzer* (Winslow et al., 2019). Meteorological variables were measured by a research-grade Campbell Scientific meteorological station deployed on the dam of FCR (Carey et al., 2022a).

2.2. High-frequency monitoring system

We monitored high-frequency light absorbance at multiple depths in FCR using a s::can Spectrolyser UV–Visible spectrophotometer (s::can Messtechnik GmbH, Vienna, Austria). This spectrophotometer was coupled with a multiplexor pumping system ('MUX' from MultiplexÔ, LLC; for technical details on the multiplexor pumping system and the sensor setup, refer to Birgand et al., 2016 and Figs. S1-S3). The MUX pumps water samples sequentially from multiple depths into a flow-through cuvette where the UV–vis absorbance spectra of the sample are measured by the spectrophotometer. The system used in our study collected measurements of light absorbance every 2.5 nm wavelengths from 200 nm to 732.5 nm (optical path length of 10 mm) approximately at an hourly time step for six monitoring depths in the reservoir.

The MUX system was used to collect high-frequency data during two time periods: reservoir turnover ("Turnover Deployment") and the initiation of HOx operation ("Oxygen On Deployment"). The Turnover Deployment captured the natural oxygenation and mixing processes that occurred during reservoir turnover and lasted from 16 October to 9 November 2020. In this study, fall turnover was defined as the onset of reservoir mixing, as determined by the first time when the temperature differential between 0.1 m and 9 m depths in the reservoir was <1 °C after summer stratification (following McClure et al., 2018, Thomas et al., 2020, and others), which occurred on 2 November 2020. During this time period the HOx system was on, so the hypolimnion was oxic before turnover, but the reservoir was thermally stratified. The Oxygen On Deployment was conducted between 26 May and 21 June 2021; during that time the HOx system was initiated on 11 June 2021 at 11:00 EDT. This deployment captured the engineered oxygenation and mixing processes resulting from the initiation of HOx operation. The HOx system induced internal mixing within the hypolimnion, but the overall thermal stratification of the reservoir was not affected. Prior to HOx operation, the reservoir was thermally-stratified and the hypolimnion was anoxic (DO < 1 mg/L); thus, while the HOx successfully added oxygen to the hypolimnion at its maximum capacity, as indicated by the transformation from soluble to total fractions of metals during activation periods (see results below), we observed a limited increase in DO concentrations due to high chemical oxygen demand, which has been

observed in many other waterbodies (Muller et al. 2012).

We took multiple steps to limit the influence of fouling of the internal components of the MUX system, due to precipitation of Fe in contact with oxygen in the measuring cuvette. Between each pump cycle, deionized water was flushed through the system. At the end of each pump sequence (one sample from each depth), dilute hydrochloric acid (5%) was automatically pumped through the system and allowed to sit in the flow-through cuvette for approximately 2 min. We also collected a reference measurement in air at the end of each cycle, which was useful in determining the extent of fouling. In addition, we switched out the cuvette every two to three days and brought the fouled one back to the lab for the following cleaning routine: soak in 50% HCl for 24 h, rinse with DI water, soak in oxalic acid for 24 h, and finally rinse with DI water. Despite these efforts, some fouling was still evident during certain time periods (see Figs. S4–5). Fouling was most pronounced in the lower wavelengths (200–250 nm; see Figs. S6–7) and therefore we removed values for wavelengths less than 250 nm before fitting PLSR models.

2.3. Sampling methods

The method seeks to create a statistical relationship between light absorbing constituents (the "color matrix") of the water with Fe and Mn concentrations. To create the calibration dataset, we sampled total and soluble Fe and Mn weekly throughout the stratified period at times and depths at which light absorbance data from the MUX-spectrometer couple were available. For this study, water samples were collected at the reservoir outtake depths of 0.1, 1.6, 3.8 m (epilimnion), 5.0 m (metalimnion), 6.2, 8.0, and 9.0 m (hypolimnion) using a 4-L Van Dorn sampler, thereby matching the MUX sampling depths. Samples for soluble Fe and Mn were syringe-filtered using 0.45 μm nylon filters. Both total and soluble metals samples were preserved with trace metal grade nitric acid to pH < 2. Samples were analyzed using Inductively Coupled Plasma Mass Spectrometry (ICPMS). Minimum reporting levels were 0.005 mg/L (Fe) and 0.0001 mg/L (Mn). The dataset, including methods for sample collection and analysis, can be found in Schreiber et al. (2022).

To assess short-term variability in metals concentrations and to calibrate and validate PLSR models, additional samples were collected every 2–4 h during two 24-hour campaigns. The first campaign occurred on 16–17 October 2020 ($n = 7$; Fig. S8); the second campaign occurred on 10–11 June 2021 ($n = 8$; Fig. S9). All sampling data (weekly and high-frequency) were used to calibrate PLSR models.

Calibration datasets were assessed for potential outliers using an ensemble approach implemented in the R package *enpls* (Xiao et al., 2019). For each model, an ensemble of 50 PLSR sub-models was generated using Monte Carlo resampling and the empirical predictive error distribution for each sample was used to identify outliers. Samples with a mean predictive error greater than three standard deviations from the mean predictive error for all samples or with a standard deviation greater than three times the mean standard deviation of all samples were considered potential outliers (Cao et al., 2017). We took a conservative approach and did not eliminate all samples that met these criteria, but rather only removed samples that were identified not only as outliers by the aforementioned method but also led to a deterioration of model fit, showed signs of sampling/analytical error, or were collected during times of cuvette fouling. After removing outliers, the calibration datasets for the Oxygen On Deployment had approximately 30% more observations than for the Turnover Deployment (Fig. 3, Table 1). Median Fe and Mn concentrations were substantially higher in the hypolimnion (6.2, 8.0 and 9.0 m) than the epilimnion (0.1, 1.6, 3.8 m) during both deployments (Fig. 3).

2.4. Predicting Fe and Mn concentrations from optical measurements using PLSR

We used PLSR to compute predictions of total and soluble Fe and Mn

Table 1
Summary of PLSR model statistics. n = number of observations. Tot. = total, Sol. = soluble. Epi = epilimnion, Hypo = hypolimnion.

Variable	Turnover Deployment							Oxygen On Deployment						
	n	PLSR Predicted Median (mg/L)	PLSR Predicted STD (mg/L)	RMSEP (mg/L)	Adj. R^2	Compo-nents	# Outliers Removed	n	PLSR Predicted Median (mg/L	PLSR Predicted STD (mg/L)	RMSEP (mg/L)	Adj. R^2	Compo-nents	# Outliers Removed
Tot. Fe (Epi)	35	0.50	0.33	0.11	0.97	5	1	47	0.50	0.10	0.07	0.73	4	1
Tot. Fe (Hypo)	34	2.23	0.99	0.53	0.84	3	2	46	2.74	1.52	1.22	0.65	4	2
Sol. Fe (Epi)	35	0.05	0.01	0.02	0.74	5	1	48	0.29	0.15	0.08	0.79	4	0
Sol. Fe (Hypo)	34	0.03	0.02	0.06	0.06	3	2	45	1.04	1.97	1.44	0.75	4	3
Tot. Mn (Epi)	36	0.23	0.19	0.06	0.97	5	0	47	0.04	0.01	0.005	0.61	4	1
Tot. Mn (Hypo)	35	0.92	0.55	0.19	0.91	4	1	46	0.56	0.16	0.14	0.58	4	2
Sol. Mn (Epi)	35	0.15	0.18	0.06	0.96	5	1	47	0.01	0.003	0.004	0.36	4	1
Sol. Mn (Hypo)	35	0.78	0.64	0.22	0.90	3	1	46	0.55	0.16	0.15	0.57	4	2

concentrations based on the correlation between absorbance spectra and sampling data. Data analysis and QA/QC was performed in the R programming environment (R.v.4.2.1). Model building was conducted using the *pls* package (Mevik et al., 2020; R Core Team 2022). The *pls* package has a built-in function for determining the number of model components based on the root mean squared error of prediction (RMSEP) using 10-fold cross validation (Mevik et al., 2020). The algorithm randomly chooses a subset of the data to be withheld for validation, while fitting the model to the rest of the data. This is repeated across 10 random segments and the RMSEP is computed for each component. RMSEP for each component is plotted against the number of components, and the number of components included in the final PLSR model is determined based on this curve. Generally, as the number of components increases, the RMSEP curve decreases sharply until reaching an inflection point where it plateaus (Fig. S18). To avoid overfitting, we chose the number of components equal to this inflection point plus or minus one, or the global minimum of the curve, whichever resulted in the lowest number of components (following Etheridge et al., 2014, Birgand et al., 2016, Mevik et al., 2020). Furthermore, it has been suggested that the number of components should not exceed 10% of the total number of observations used to calibrate the model (Mevik et al., 2020). We followed this rule to the greatest extent possible. In some cases, the number of components slightly exceeded the 10% requirement, but this only occurred when including an additional component would substantially decrease the RMSEP determined by 10-fold cross validation, while also improving the variance explained by the model. Given the sensitivity of the PLSR method, our approach was to optimize the tradeoff between model fit and predictive accuracy. Once the number of components was determined, the model was fit to the observational data and predictions were made using the high-frequency absorbance measurements. In some cases, PLSR predicted slightly negative concentration values. For the purposes of this analysis, we considered negative values to have a value of 0 mg/L for all variables, unless stated otherwise.

Separate PLSR models were developed for each variable (total Fe, soluble Fe, total Mn, and soluble Mn) and deployment. Based on the distinctly different chemical and biological characteristics between layers of the reservoir (i.e., epilimnion and hypolimnion), we found that the best fit was obtained when we used different models for the two layers. In stratified reservoirs such as FCR, Fe and Mn concentrations are higher in the hypolimnion than the epilimnion (see Fig. 3). Therefore, we had an epilimnion model which included data from 0.1, 1.6, and 3.8 m and a hypolimnion model which included data from 6.2, 8.0, and 9.0 m (Table 1). Although we also collected data from 5.0 m, we did not include them in our analyses since this is at the transition between the two layers (metalimnion; see McClure et al., 2018) and thus not applicable to either layer. We developed separate models for the Turnover Deployment and the Oxygen On Deployment. In the end, we had four separate models for each of the four variables (total and soluble Fe and Mn), resulting in 16 different models.

To assess the uncertainty of the predictions made using PLSR, we calculated nonparametric bootstrap predictive intervals following methods described by Denham (1997). Briefly, a model was first fit to the available observational data (Y) and absorbance spectra (X) using the predetermined number of components. This model was used to make predictions (E). Then, the residuals of the original model were randomly sampled and added to Y and E to obtain a new set of values for the dependent variable, denoted here as Y', and new predictions, denoted here as E'. A new model was fit to X and Y', and again used to make new predictions (Ê'). The prediction error was then calculated based on E' - Ê'. This process was repeated 1000 times to obtain the bootstrapped error distribution (G). We then calculated the 0.05 and 0.95 quantiles of G, which represented the 90% predictive intervals around the predictions from the original model (Denham 1997).

Model skill was assessed using the coefficient of determination (R^2) from the linear regression between predicted and observed values, as well as the root mean squared error of prediction (RMSEP) for each model (following Wold et al., 2001 and Mevik et al., 2020).

All observational data, including the spectrophotometer data, are published in the Environmental Data Initiative repository (Carey et al., 2022a; Carey et al., 2022b; Carey et al., 2022c; Schreiber et al., 2022, and Hammond et al., 2023). All code used to analyze the spectrophotometer data with PLSR and generate the figures is available in the Zenodo repository (Hammond 2022).

3. Results

3.1. Routine Fe and Mn sampling trends

Weekly sampling at FCR showed levels of Fe and Mn in exceedance of the EPA standards during the 2020 and 2021 stratified periods, with maximum total Fe and Mn concentrations of 18.5 mg/L and 2.2 mg/L, respectively (Fig. 2). Hypolimnetic concentrations of both metals generally increased throughout the summer stratified period of each year, until reservoir fall turnover (Fig. 2). Following reservoir turnover, concentrations of both metals remained < 1 mg/L until the following spring (Fig. 2).

3.2. PLSR model performance

A comparison of skill metrics among the 16 models revealed that PLSR performed best for models calibrated with Fe and Mn concentrations greater than 0.03 mg/L (Tables 1, S1; Fig. S10). Model skill was also sensitive to the number of components included in each model. For the Turnover Deployment, the number of components included in the PLSR models ranged from 3 to 5 (9–14% of n). For the Oxygen On Deployment, 4 components were used for all PLSR models (8–9% of n) (Table 1). Sample size was negatively correlated with R^2, but positively correlated with RMSEP (Fig. S10).

Turnover Deployment models explained a high proportion of the variability in total and soluble Fe and Mn concentrations ($R^2 = 0.74$ to 0.97), excluding hypolimnetic soluble Fe which had a poor model fit ($R^2 = 0.06$), likely due to low concentrations (median = 0.02 mg/L) (Table 1; Fig. 3). In comparison, Oxygen On Deployment models explained a lower proportion of the variability in total and soluble Fe and Mn concentrations ($R^2 = 0.57$ to 0.79), with one model of epilimnetic soluble Mn having an R^2 of 0.26, likely due to low concentrations (median = 0.01 mg/L) (Table 1). PLSR model performance also varied between the hypolimnion and epilimnion. For most models, the epilimnetic PLSR model had a higher R^2 value than the corresponding hypolimnetic PLSR model (Table 1).

In most cases, PLSR predictions were within the range of concentration values in the calibration dataset (Figs. 3, S11–12), but they did not capture some of the high-magnitude fluctuations in the sampling data. Analysis of the Fe and Mn time series (Figs. 4D-E and 5D-E) and calibration (Figs. S11–12) suggests that inaccuracy in the models was largely attributed to calibration error for observations far from the mean concentration of the calibration data (i.e., outliers). Additionally, when predicting variables with low concentrations (< 0.03 mg/L), especially with the epilimnion models, some predictions were in the negative range (Figs. 4D-E; 5D-E).

3.3. Reservoir turnover deployment

3.3.1. Water temperature, stratification, and DO concentrations

DO concentrations, water temperature, and Schmidt stability varied considerably over the course of the Turnover Deployment (Fig. 4A-C). Prior to turnover, DO concentrations were strongly stratified by depth and exhibited large sub-daily fluctuations in the epilimnion and metalimnion (Fig. 4C). Hypolimnetic DO concentrations were stable around 2 mg/L during the pre-turnover period, due to the HOx system operation (Fig. 4C). A sharp temperature gradient (4–7 °C) between the epilimnion

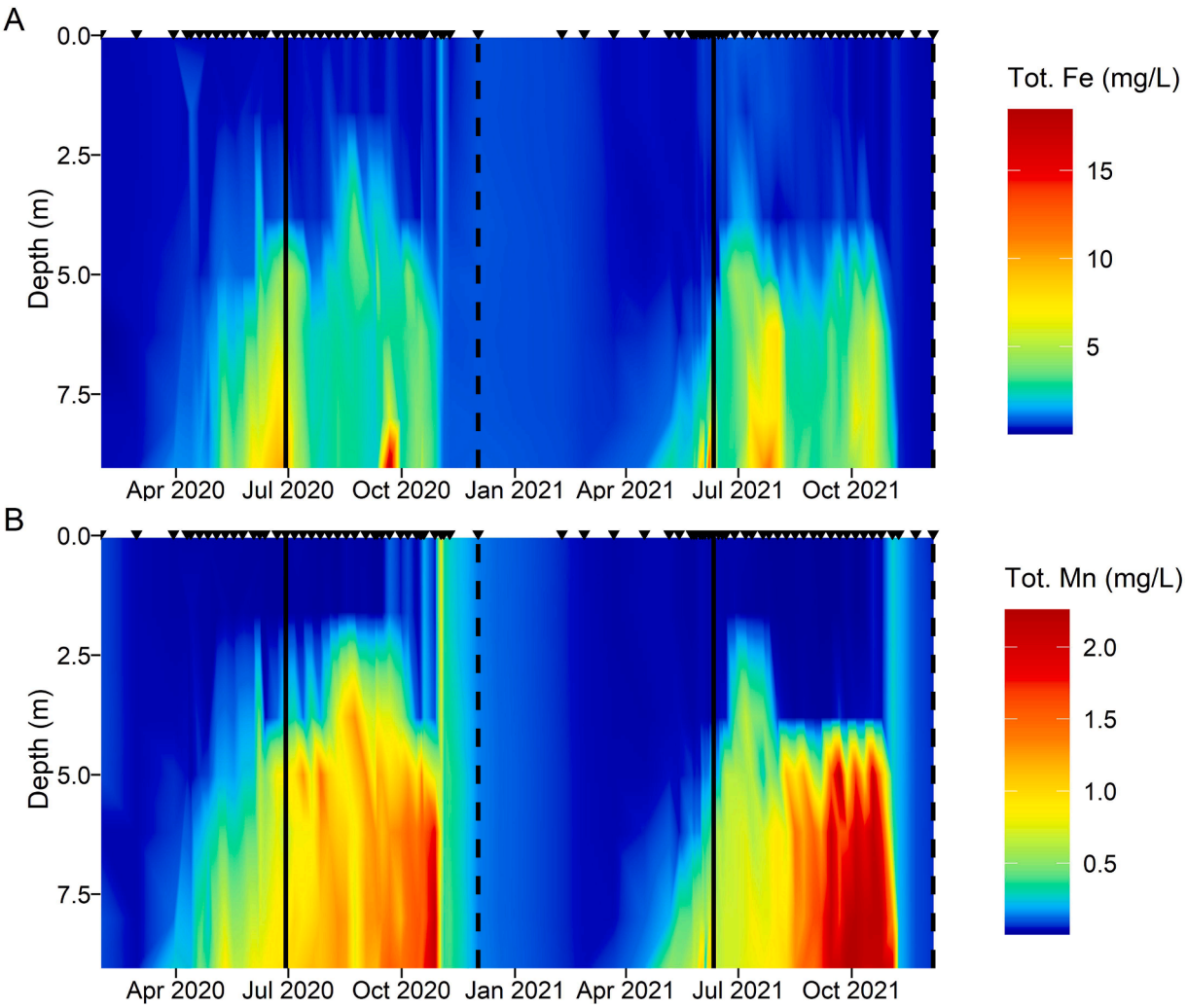

Fig. 2. A) Total Fe and B) total Mn concentrations in FCR from 2020 until 2021. Total Fe and Mn concentrations are derived from manual samples that are collected approximately weekly during the summer stratified period each year. The HOx system was activated on 29 June 2020 and 11 June 2021 (solid black vertical lines) and deactivated on 02 December 2020 and 06 December 2021 (dashed black vertical lines). Values are linearly interpolated for plotting purposes. Inverted triangles at the top of the panel indicate sampling times.

and hypolimnion existed until approximately 3 days prior to turnover (Fig. 4B). However, the water temperature profile equalized periodically between the metalimnion and hypolimnion prior to turnover, indicating ephemeral periods of mixing between those layers (Fig. 4B). Starting on 29 October 2020, the temperature gradient decreased progressively until the full water column temperature profile equalized on 02 November 2020, meeting our criteria for turnover.

3.3.2. *Predicted Fe and Mn concentrations*

Reservoir turnover had substantial impacts on Fe and Mn concentrations. At the beginning of the deployment (16 October 2020), 17 days prior to turnover, both Fe and Mn displayed large differences in concentration between the epilimnion and hypolimnion (Fig. 4D-E). The average total Fe and total Mn concentrations across all hypolimnetic depths (6.2, 8.0, and 9.0 m) were 3.73 mg/L and 1.48 mg/L; across all epilimnetic depths (0.1, 1.6, and 3.8 m) they were 0.41 mg/L and 0.14 mg/L, respectively (Fig. 4D-E). Substantial changes in epilimnetic concentrations were not observed until 24 h prior to turnover. Within that 24 hour period, average epilimnetic total Fe and total Mn increased by 70% (0.61 to 1.04 mg/L) and 66% (0.29 to 0.48 mg/L), respectively.

In contrast to the epilimnion, we observed declining total Fe and Mn concentrations in the hypolimnion prior to turnover (Fig. 4D-E). Between 16 October and 02 November 2020, hypolimnetic total Fe and total Mn concentrations declined at a rate of 0.13 and 0.11 mg/L/d, respectively. However, there were also periods of fluctuations in total Fe and total Mn concentrations by as much as 1 mg/L/d (Fig. 4D-E). In the 24 h prior to turnover, average hypolimnetic total Fe and total Mn decreased by 45% (2.09 to 1.14 mg/L) and 32% (0.82 to 0.55 mg/L), respectively.

A strong concentration gradient between the epilimnion and hypolimnion remained for total Fe and total Mn until full reservoir turnover on 02 November 2020. After turnover, water temperature and DO rapidly equalized across the full water column, coinciding with the rapid equalization of total Fe and Mn concentrations across the water column (Fig. 4D-E). Total Fe and Mn concentrations decreased and were less variable than during the pre-turnover period (Fig. 4D-E). The reservoir remained well-mixed for 2 days, but then shifting thermal gradients led to a temporary re-stratification that began on 02 November 2020 and lasted until the end of the deployment on 09 November 2020 (Fig. 4A-B). The re-stratification of the reservoir was also evident in total Fe and total Mn concentrations (Fig. 4D-E).

3.4. *Oxygen on deployment*

3.4.1. *Water temperature, stratification, and DO*

DO concentrations, water temperature, and Schmidt stability

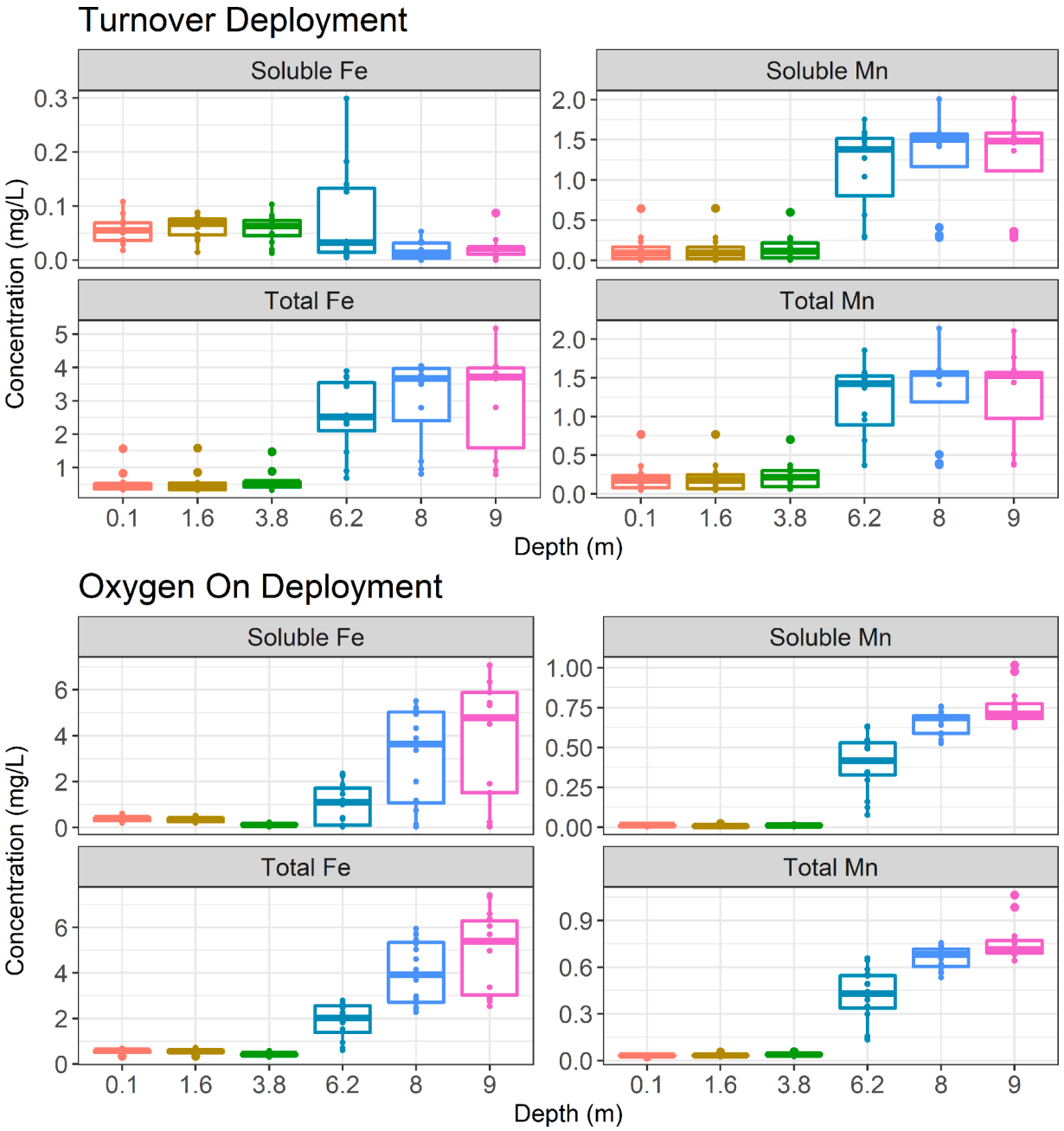

Fig. 3. Sampling data used to calibrate PLSR models for the Reservoir Turnover Deployment ($n = 69$ for total and soluble Fe, 71 for total Mn, and 70 for soluble Mn) and the Oxygen On Deployment ($n = 93$ for all variables). Outliers (determined by the Monte Carlo predictive error distribution) are not included. Note that the y-axes vary among panels.

differed considerably between the two deployments (Fig. 5A-C). At the start of the Oxygen On deployment (26 May 2021), 16 days prior to HOx activation, epilimnetic DO concentrations were high (5–15 mg/L) and exhibited a consistent decline throughout the deployment due to warm air temperatures (Fig. S14). Metalimnetic and hypolimnetic DO concentrations were both approximately 0 mg/L throughout the deployment. The water temperature profile shows distinctly stratified layers in the reservoir prior to HOx operation, with a sharp temperature gradient throughout the epilimnion for the entire deployment and a slight temperature gradient in the hypolimnion (Fig. 5B). Immediately following HOx activation on 11 June 2021, the water temperature profile equalized across layers below 6 m depth, indicating mixing within the hypolimnion due to HOx activation (Fig. 5B). The water temperature profile in the epilimnion was unaffected by HOx operation. Metalimnetic and hypolimnetic DO concentrations did not increase above 0 mg/L in the few days after activation of the HOx system. This is attributed to chemical oxygen demand in the hypolimnion resulting from elevated concentrations of reduced solutes (e.g., Fe(II) and Mn(II)).

3.4.2. *Predicted Fe and Mn concentrations*

At the beginning of the deployment, the highest concentrations of total Fe and Mn were at the lowest depth (9 m) and concentrations decreased upwards in the water column, with a sharp decrease between the hypolimnion and epilimnion (Fig. 5D-E). In the first 24 h of the deployment, total Fe and Mn concentrations averaged across all epilimnetic depths were 0.43 and 0.03 mg/L, respectively, while across the hypolimnetic depths they were 2.71 and 0.54 mg/L, respectively. Prior to HOx operation, both total Fe and Mn in the hypolimnion exhibited

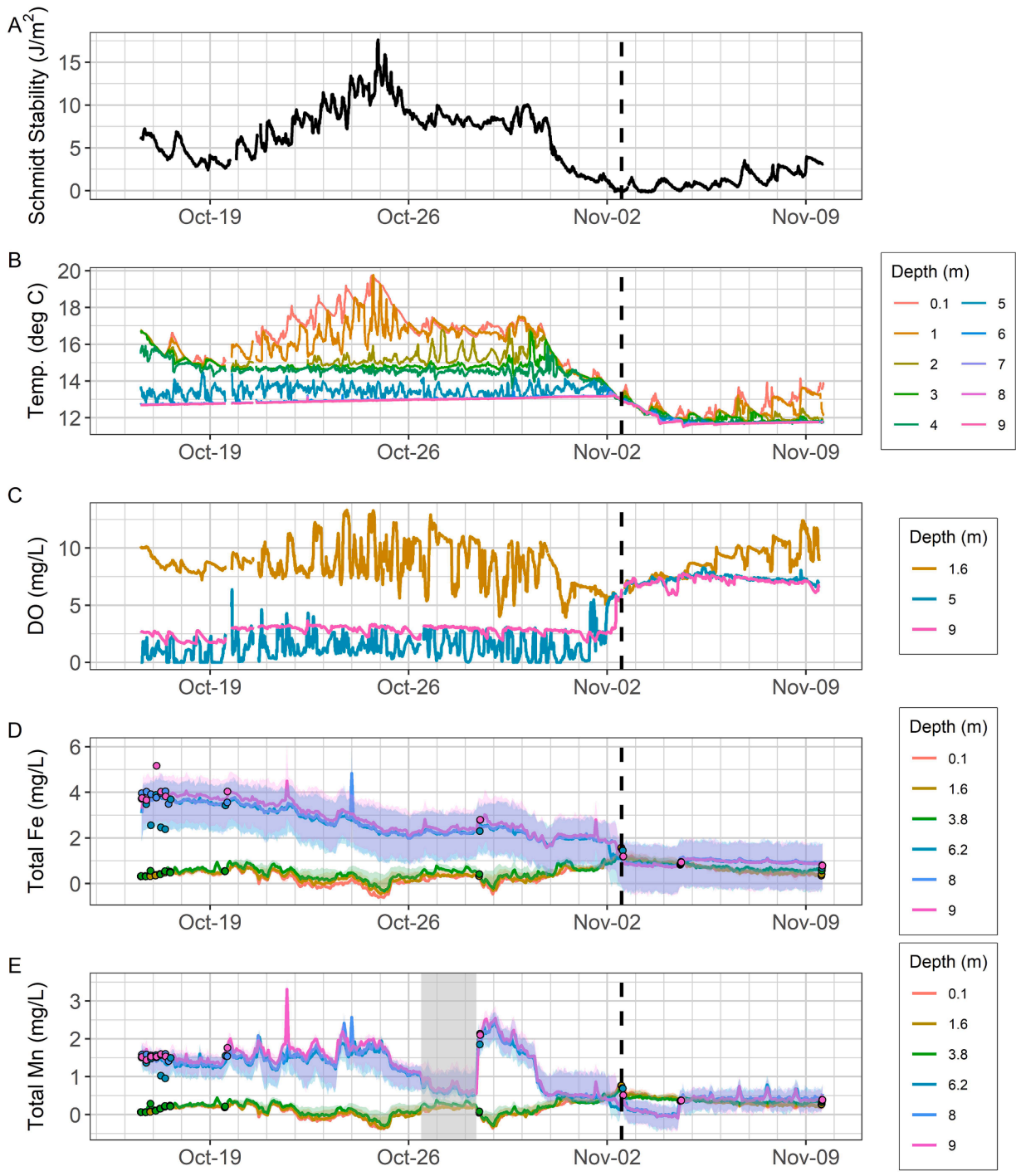

Fig. 4. Time series plots of A) Schmidt stability, B) water temperature, C) dissolved oxygen, D) predicted total Fe concentrations (lines) with observed values (dots) and 90% predictive intervals (shaded areas), and E) predicted total Mn concentrations (lines) with observed values (dots) and 90% predictive intervals (shaded areas) during the Reservoir Turnover Deployment. The dashed vertical line on 02 November 2020 represents reservoir turnover (see text for definition). Shaded area in late October shows region of lower uncertainty of Mn predictions due to possible cuvette cleaning issues. Colors of lines (PLSR predictions) and dots (samples) are shown on the color scale to the right. Note that the reservoir temporarily re-stratified after 02 November 2020. Time series plots for soluble Fe and Mn are shown in Fig. S16.

large, sub-daily fluctuations which resulted in concentration changes of up to 1.62 mg/L/hr and 0.19 mg/L/hr, respectively (Fig. 5D-E). These sub-daily fluctuations were most pronounced at the lowest depth.

The spatial and temporal dynamics of Fe and Mn concentrations were significantly affected by hypolimnetic oxygenation. Prior to activation of the HOx system on 11 June 2021, epilimnetic total Fe and Mn concentrations remained constant (sd = 0.07 mg/L and 0.004 mg/L, respectively) and had maximum concentrations of 0.63 mg/L and 0.05 mg/L, respectively. Hypolimnetic total Fe and Mn concentrations during this period were much more variable (sd = 1.85 mg/L and 0.19 mg/L, respectively) with maximum concentrations of 7.90 mg/L and 1.08 mg/L, respectively. Shortly after HOx activation, total Fe and Mn concentrations equalized contemporaneously with the equalization of water temperature across the hypolimnetic depths, indicating that this layer of the reservoir was well-mixed with respect to Fe and Mn (Fig. 5B, 5D-E). In contrast, differences in total Fe and Mn concentrations across the epilimnetic depths increased slightly after activation of the HOx system.

Approximately 6 h after turning on the HOx system, total Fe and Mn

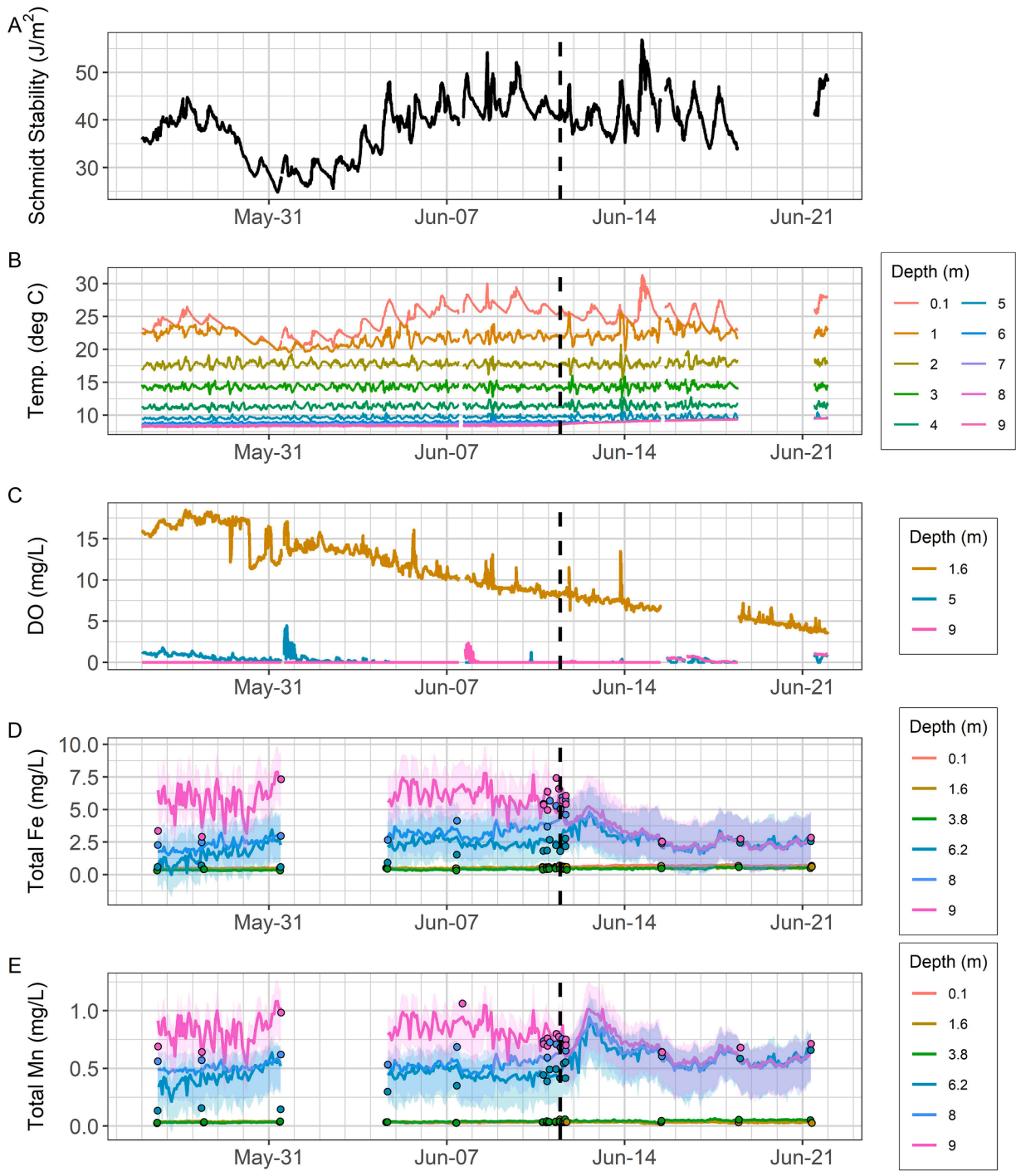

Fig. 5. Time series plot of A) Schmidt stability, B) water temperature, C) dissolved oxygen, D) predicted total Fe concentrations (lines) with observed values (dots) and 90% predictive intervals (shaded area), and E) predicted total Mn concentrations (lines) with observed values (dots) and 90% predictive intervals (shaded areas) during the Oxygen On Deployment. The dashed vertical line represents the time that the HOx was turned on. Time series plots for soluble Fe and Mn are shown in Fig. S17. Note that the MUX was not collecting data from 11:00 EDT 31 May 2021 until 14:30 EDT 4 June 2021 due to technical issues. Gaps in DO and water temperature data are due to sensor malfunction and/or maintenance.

at 9 m depth declined by approximately 2.5 mg/L and 0.25 mg/L, respectively (Fig. 5D-E). Concentrations of total Fe and Mn at all hypolimnetic depths subsequently increased over the next 24 h, before eventually stabilizing over the following 24 h at concentrations of 1.5–3.5 mg/L and 0.5–0.75 mg/L, respectively. For the remainder of the deployment, total Fe and Mn concentrations remained equal across all hypolimnetic depths and exhibited less variability (Fig. 5D-E).

3.5. Predicted Fe and Mn soluble-to-total ratios

The ratio of predicted soluble to total Fe (SFe:TFe) and Mn (SMn:TMn) was calculated to assess redox transformations. We observed distinct changes in these ratios over the course of both deployments, most notably in the hypolimnion (Fig. 6). During the Turnover Deployment, the hypolimnion was maintained at oxic conditions pre-turnover (due to HOx) and post-turnover (due to mixing). As expected, hypolimnetic SFe:TFe was approximately 0 during this entire

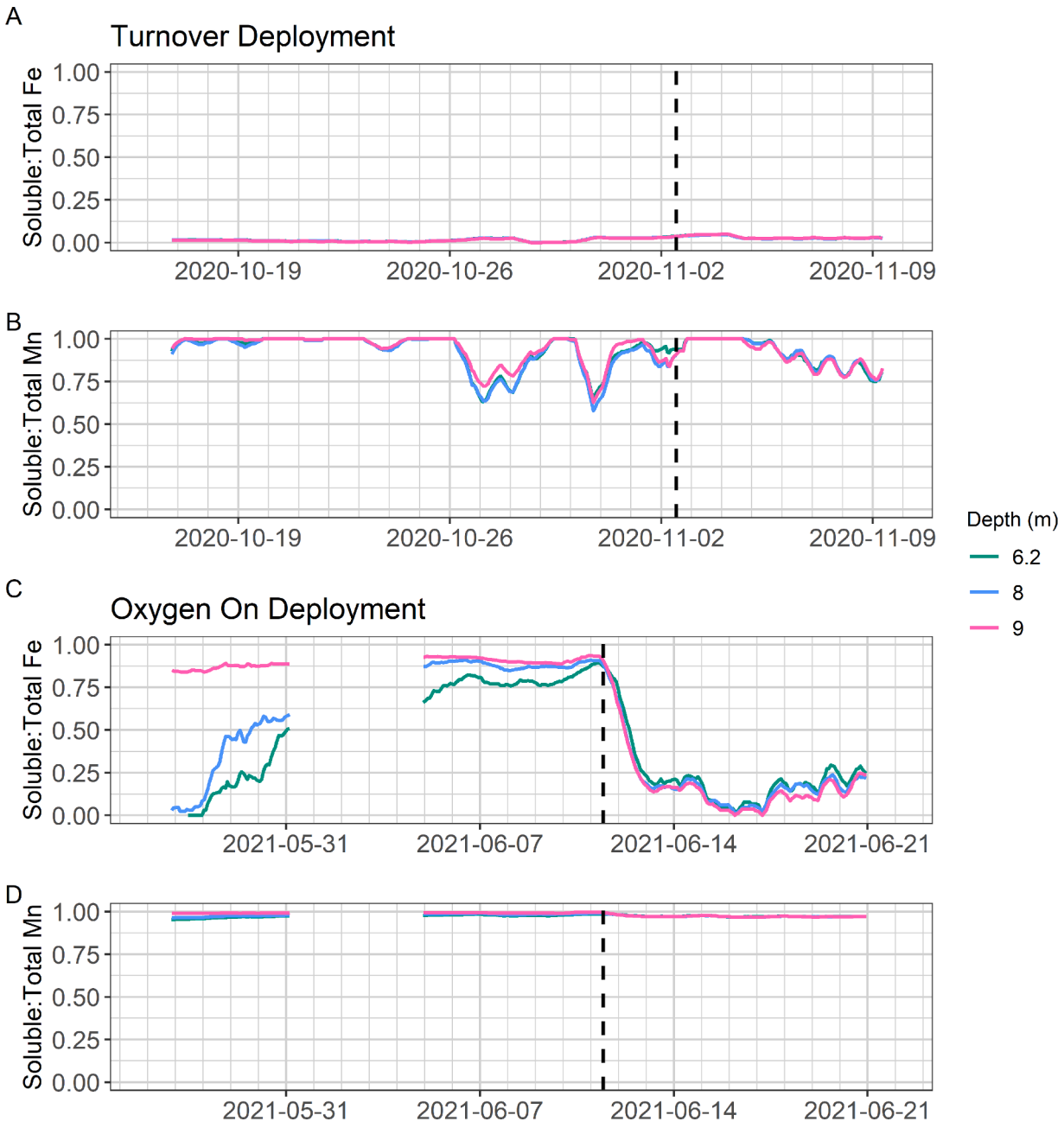

Fig. 6. A) the ratio of predicted soluble Fe to total Fe and B) the ratio of predicted soluble Mn to total Mn in the hypolimnion during the Turnover deployment; C) the ratio of predicted soluble Fe to total Fe and D) the ratio of predicted soluble Mn to total Mn in the hypolimnion during the Oxygen On Deployment. Values were smoothed with a 10-hr moving average to remove noise. The dashed vertical lines represent the times when reservoir turnover occurred in panels A-B and when the HOx system was turned on in panels C-D. PLSR predictions that had negative values were set to zero when calculating ratios and any ratio value that was greater than 1 was set to 1. Note that the MUX was not collecting data from 11:00 EDT 31 May 2021 until 14:30 EDT 4 June 2021 due to technical issues.

deployment, indicating that all Fe in the hypolimnion was in the particulate fraction (soluble Fe + particulate Fe = total Fe). In contrast, hypolimnetic SMn:TMn was approximately 1 at the beginning of the deployment, indicating that all Mn was in the soluble fraction. However, in the week prior to turnover, hypolimnetic SMn:TMn oscillated between 0.5 and 1. Following turnover, SMn:TMn remained greater than 0.75 until the end of the deployment.

At the beginning of the Oxygen On deployment, SFe:TFe differed greatly with depth in the hypolimnion, with ratios greater than 0.8 at 9 m depth and ratios close to 0 at 6.2 m and 8 m depths (Fig. 6C-D). Between the beginning of the deployment and HOx activation on 11 June 2021, the SFe:TFe at 6.2 m and 8 m increased continuously to approximately the same level as 9 m (Fig. 6C-D). Just before the initiation of HOx operation, the SFe:TFe at all hypolimnion depths was > 0.75, indicating that most of the Fe in the hypolimnion was in the soluble fraction. However, immediately after turning the HOx system on, the SFe:TFe in the hypolimnion decreased steadily. In the 48-hour period after HOx activation, the SFe:TFe in the hypolimnion declined to less than 0.25 until the end of the experimental period (Fig. 6C-D), indicating oxidation processes. In contrast to Fe, SMn:TMn in the hypolimnion was > 0.90 for the entire deployment. We did not observe a significant effect of HOx operation on SMn:TMn (0.99 pre-HOx, 0.97 post-HOx).

4. Discussion

4.1. PLSR modeling of high frequency absorbance spectra can predict Fe and Mn concentrations

Using UV-visible absorbance spectra and PLSR modeling, we made hourly predictions of Fe and Mn concentrations at 6 depths in our study reservoir. Our results indicate that this method can successfully predict Fe and Mn concentrations, with some limitations (discussed below), based on their covariability with UV–vis absorbance spectra, despite the paucity of clearly-defined absorbance peaks for these elements. PLSR models were able to explain a high proportion of the variability in the sampling data (see R^2 values in Table 1) and predictions agreed with expected trends in Fe and Mn concentrations. For example, the rapid decline in SFe:TFe following the onset of HOx operation (Fig. 6C) matches expectations based on the rapid oxidation kinetics of Fe(II) in the presence of oxygen (Davison and Seed 1983); previous studies have also demonstrated substantial decreases in soluble Fe following short periods of HOx (Dent et al., 2014; Munger et al., 2016; Krueger et al., 2020). Based on model skill metrics (i.e., R^2 and RMSEP) and visual inspection of the predicted time series, accurate predictions of Fe and Mn concentrations using this method are influenced by numerous factors, including: the range and variance of concentrations in the calibration dataset, the sample size used for calibration, the number of outliers in the calibration dataset, the number of components in the PLSR model, and the inherent predictability of each variable at a particular site (i.e., the strength of correlation with the UV–vis absorbance spectra).

Our results suggest that our methodology may be most appropriate for measuring elevated concentrations of Fe and Mn ($>$ 0.1 mg/L). This result agrees with Vaughan et al. (2018), who suggested that the application of this method to predict riverine total phosphorus (TP) concentrations was best for sites with elevated TP ($>$ 0.1 mg/L) concentrations. In our study, PLSR models fit to data with concentrations of Fe and Mn ($<$ 0.03 mg/L) generally did not perform well. For example, soluble Fe during the Turnover Deployment had median concentrations of 0.02 mg/L in the hypolimnion (Fig. 3 and Table S1). Accordingly, the PLSR models for hypolimnetic soluble Fe had the lowest R^2 (0.06) and highest RMSEP relative to median calibration concentration out of any model for the Turnover Deployment (Tables 1, S1).

Our PLSR models were also sensitive to the range and variance of sampling data used for calibration. Preliminary model testing revealed that PLSR models were hindered by the distinct water chemistry between epilimnetic and hypolimnetic depths (Fe and Mn mean differences $>$1.3 mg/L and 0.8 mg/L, respectively; see Fig. 3) and therefore models were generated separately for each reservoir layer. This conforms with findings of previous studies using in situ UV–vis spectrophotometers and PLSR in waterbodies, which all achieved higher accuracy with site-specific models (Avagyan et al., 2014; Vaughan et al., 2018; Etheridge et al., 2014). However, when comparing pairs of PLSR models (i.e., the same variable + depth combination) between the two deployments, the models fit to data with a higher standard deviation had higher R^2 values, with the sole exception of hypolimnetic total Fe (Tables 1 and S1). These results suggest that there is a tradeoff between capturing the maximum variability in observed concentrations and the limitations imposed by the degree of covariability between the UV–vis absorbance spectra and the variable of interest (also observed by Avagyan et al., 2014 and Allen 2021). To achieve an accurate predictive model, grouping data based on the spatial and temporal context of measurement achieved a better fitting model while still maximizing the variability captured in the calibration data.

Birgand et al. (2016) used a similar approach for making predictions of soluble Fe concentrations in FCR after the activation of a HOx system. They obtained a slightly better model fit, indicated by an R^2 value of 0.94, compared to our R^2 values of 0.79 and 0.75 (epilimnion and hypolimnion, respectively) for the Oxygen On Deployment. We used calibration sample sizes of 48 and 45 (epilimnion and hypolimnion, respectively) while Birgand et al. (2016) used 27. However, they used 5 components in their PLSR model, whereas we used 4 components. Thus, the higher R^2 value for their model may be attributed to a higher ratio of components to sample size (18%) compared to our study (8–9%), which has been shown in other applications of PLSR (Mevik et al., 2020; Etheridge et al., 2014; Birgand et al., 2016).

Our results captured sub-weekly patterns in Fe and Mn dynamics in FCR, but the PLSR-predicted time series of Fe and Mn concentrations was not able to adequately capture some of the high-magnitude, sub-daily fluctuations that were observed in the sampling data (Figs. 4 and 6). This is likely due to varying PLSR model skill, which is related to the sample size and distribution of data used for calibration, the number of PLSR model components, and the inherent predictability of each variable. Therefore, it follows that the strength of correlation between the UV–vis absorbance spectra and Fe/Mn concentrations plays a strong role in determining the limits to the temporal resolution. This relationship can be refined through the methodological suggestions outlined below, but ultimately depends upon the spectral properties of the study system.

There are several limitations of this method that should be addressed in future research. In our reservoir, the cuvette fitted on the spectrophotometer experienced fouling, likely due to Fe and Mn in the hypolimnion that oxidized and precipitated on the cuvette walls upon exposure to oxygen. Despite our efforts to limit fouling (see Methods), there was still a fouling signal detected in several periods of our time series. Although fouling occurred, the PLSR models still provided a remarkably good numerical correction for this fouling signal. For future work, we recommend collection of additional calibration samples obtained at regular intervals between servicing dates as this will give a chance for the PLSR model to correct for the timing and kinetics of the optics fouling and may thus lower uncertainties. We also found that truncating the UV–vis absorbance spectra used for calibration to only include wavelengths greater than 250 nm substantially improved the model skill and diminished spikes in the time series of predictions that corresponded to periods of heavy fouling (Figs.S6 and S7). Finally, we focused this study on high frequency measurements over a short term (day to week) and not on long-term (month to year) predictions. Additional work would need to be done, with longer deployments and calibration data, to establish if longer-term predictions can be made.

4.2. Fe and Mn concentrations change gradually in response to weakening stratification and rapidly in response to fall turnover

Trends in predicted Fe and Mn concentrations shed light on the changes that occurred in the reservoir before and after turnover. Hypolimnetic concentrations of Fe and Mn began declining 17 and 9 days prior to turnover, respectively, and shorter periods of more rapid concentration fluctuations were superimposed upon these patterns of decline (Fig. 4D-E). Combined, these results suggest that turnover, at least in our study reservoir, is not a discrete event, but rather a process occurring over an extended time period. McMahon (1969) measured a similar decrease in soluble Fe using daily samples for nine days across spring mixing in a dimictic lake; soluble Fe concentrations decreased by more than one order of magnitude 5 days prior to full circulation. McMahon (1969) did not offer any interpretation of this phenomenon, simply stating that the changes in soluble Fe were concurrent with vernal circulation. Similar trends have also been observed in other parameters of biogeochemical relevance. For example, Kankaala et al. (2007) found that the majority of CH_4 in the hypolimnion of a lake was microbially oxidized at the oxycline boundary during a month-long period of weakening stratification before complete mixing occurred, resulting in lower effluxes of CH_4 to the atmosphere during turnover.

Predicted Fe and Mn concentration data can be compared to other time series data to infer mechanisms behind the declining Fe and Mn concentrations prior to turnover. Based on trends in Schmidt stability and water temperature (Fig. 4A-B), reservoir stratification was

weakening for a 9-day period prior to full turnover, in response to daily and hourly shifts in meteorological conditions, including air temperature and wind speed (Fig. S13). Mixing between the hypolimnion and metalimnion, as indicated by the homogenization of water temperature between these layers, occurred periodically throughout the deployment, with an increasing frequency as turnover approached (Figs. 4A-B, S15). These ephemeral periods of mixing between the hypolimnion and metalimnion likely led to exchange of Fe and Mn between layers, which suggests that hydrodynamic processes occurring on hourly to daily time scales may have a substantial influence of Fe and Mn cycling. However, without Fe and Mn concentration data at a high spatiotemporal resolution, these patterns would not be observed.

The flexibility of using a multiplexor-spectrophotometer system with a customized prediction algorithm (e.g., site-specific PLSR models) allows for the quantification of high-resolution elemental stoichiometry by making predictions of both the soluble and total fractions of Fe and Mn. During the Turnover Deployment, Fe was predominantly composed of the total fraction, whereas Mn was largely composed of the soluble fraction until approximately one week before turnover, at which time the SMn:TMn ratio began to decline (Fig. 6B). This coincided with the onset of declining total Mn concentrations that continued until turnover, excluding a 2-day period from 28 October to 30 October 2020 when total Mn concentrations temporarily increased (Fig. 4E). The shift to declining SMn:TMn and total Mn concentrations also coincided with increased frequency of mixing between the metalimnion and hypolimnion and declining stratification intensity (Figs. 4A-B and 6B). These trends suggest that declining total Mn concentrations in the pre-turnover period were the result of increased oxidation of Mn(II), perhaps due to the exposure of Mn(II) in the hypolimnion to Mn-oxidizing microbes that inhabit the metalimnion, as demonstrated by a previous study at FCR showing that the presence of Mn-oxidizing microorganisms can substantially increase Mn oxidation rates (Munger et al., 2016).

4.3. *Hypolimnetic oxygenation causes rapid oxidation of Fe, with lesser impact on Mn*

The MUX-spectrophotometer system enabled us to observe Fe and Mn concentration changes in response to hypolimnetic oxygenation at an unprecedented spatiotemporal resolution. Fe and Mn concentrations in the hypolimnion both spiked in the 48 h following oxygenation, then declined (Fig. 5D-E). However, Fe concentrations decreased to levels lower than they were prior to oxygenation, especially at the lowest depth, whereas Mn concentrations declined to approximately the same levels prior to oxygenation (Fig. 5D-E). These results suggest that the HOx system physically mixed the hypolimnion with respect to both metals, as total Fe and total Mn concentrations quickly converged across hypolimnetic depths after turning on the HOx system (Fig. 5D-E). The physical mixing induced by the HOx system appeared to affect Fe and Mn similarly, suggesting that the spike in total Fe and Mn immediately following HOx activation was a result of increased mixing and/or entrainment of particulates in the hypolimnion due to stirring of the bottom sediments. The convergence of Fe and Mn concentrations across hypolimnetic depths has previously been observed in response to HOx activation (Gerling et al., 2014), but results from this study reveal that this can occur in less than 24 h, and may subsequently be followed by an ephemeral spike in total Fe and Mn concentrations.

Concentrations of total Fe and Mn displayed more short-term variability prior to HOx activation than they did post-activation. This was especially pronounced at the lowest depth (9m) where concentrations fluctuated significantly over a period of less than 24 h (Fig. 5D-E). Given that the SFe:TFe ratio in the upper and middle hypolimnion (6.2 m and 8 m) steadily increased during the pre-HOx period (Fig. 6C), likely due to diffusion of soluble Fe out of the lower hypolimnion, the rapid fluctuations in total Fe in the lower hypolimnion may have been attributed to shifting diffusion gradients. However, similar patterns in short-term variability were observed in Fe and Mn, despite the fact that Mn was predominantly in the soluble phase for the entire deployment, suggesting that diffusion of soluble Mn out of the lower hypolimnion was not responsible for the pre-HOx rapid fluctuations observed at 9 m.

The change in redox conditions caused by adding DO to the hypolimnion had a much more pronounced effect on Fe than Mn, as has been observed in other studies (e.g., Gantzer et al., 2009). The contrasting responses of Fe and Mn to oxygenation can be seen most clearly in the resulting changes in soluble:total ratios (Fig. 6). The SFe:TFe ratio in the hypolimnion exhibited a nearly constant linear decline in the 48 h post-oxygenation and remained below 0.25 for the remainder of the deployment. This indicates that soluble Fe in the water column was rapidly oxidized by the HOx system, even though there was no measurable increase in hypolimnetic DO. This is further supported by the fact that the mean hypolimnetic total Fe concentration was consistently lower after HOx operation began than it was previously. The observed trends in SFe:TFe ratios agree with previous research on the effects of HOx systems on Fe in lakes and reservoirs. For example, Dent et al. (2014) found that SFe:TFe declined to 0.58 after 8 h of hypolimnetic oxygenation. In our study, it took approximately twice as long (16 h) for SFe:TFe to reach 0.58. However, the Fe concentrations in Dent et al. (2014) were lower (0.17 - 2.88 mg/L) than those in our study (0.31 - 7.42 mg/L).

In contrast to Fe, the SMn:TMn ratio in the hypolimnion displayed only a very slight response (approximately 2% decrease) to HOx activation, demonstrating that hypolimnetic oxygenation did not result in significant oxidation of Mn at the timescale of our deployments. Our results agree with those from Dent et al. (2014), who found that Mn was still 100% in the soluble phase 8 h after oxygenation. Furthermore, previous studies at FCR have also showed that soluble Mn does not respond significantly to oxygenation alone and that other factors, such as microbially-mediated oxidation, reservoir pH (range 6.4 - 7.1 observed in the hypolimnion during our study), sorption and dilution from physical mixing, are more important variables impacting hypolimnetic soluble Mn than oxygenation (Munger et al., 2016; Krueger et al., 2020).

5. Conclusions

Results from this study demonstrate that coupling a spectrophotometer with a multiplexed pumping system enabled high-frequency monitoring of Fe and Mn at multiple depths in our study reservoir, providing a unique ability to observe hour-resolution biogeochemical dynamics in a freshwater ecosystem. Although there are limitations to the method, our findings confirm that it is possible to correlate the “color matrix” (light absorbance rich data) of water to parameters not known to absorb light, using a site-specific statistical calibration (PLSR) to unveil processes tightly-coupled in space and in time. Our results underscore the importance of implementing robust and consistent methodologies for obtaining calibration concentrations, choosing the number of components in PLSR models, and quantifying the uncertainty around predictions.

The high-spatiotemporal resolution predictions provide novel insights into Fe and Mn dynamics that could improve aquatic monitoring programs and reservoir management practices. First, we demonstrated that Fe and Mn concentrations can fluctuate significantly on time scales much shorter than those employed by most traditional monitoring programs. For example, sub-daily fluctuations of total Fe and Mn during the Oxygen On Deployment resulted in concentration changes of up to 1.62 mg/L/hr and 0.19 mg/L/hr, respectively. Considering that the secondary drinking water standards for Fe and Mn are 0.3 and 0.05 mg/L, respectively, sub-daily concentration changes of this magnitude are critical for water quality management. Second, we observed an increase in total hypolimnetic Fe and Mn in response to the re-stratification of our study reservoir two days after turnover, which contradicts the common assumption that metals concentrations equalize and decrease during the mixed period following turnover. Last, our results offer new insights on

the rapid response of Fe to hypolimnetic oxygenation; within hours of activating the system, the soluble to total Fe ratio indicated oxidation of Fe, even though there was no measurable increase in DO. This study emphasizes the power of high spatiotemporal resolution data for improving our understanding of biogeochemical cycles by unveiling previously-unobserved processes altering Fe and Mn concentrations.

Authorship statement

NWH, FB, and MES co-conceived the design of the study. NWH led field sampling, and MES, BB, and ABP assisted in field sampling. FB, CCC, and BB conducted the initial field testing for the MUX and development of the PLSR analysis workflow. ABP led the collection of auxiliary sensor data. NWH, FB, CCC, and MES led conceptual development and writing.

Declaration of Competing Interest

The authors declare the following financial interests/personal relationships which may be considered as potential competing interests: Carey, Brigand, Schreiber report financial support was provided by National Science Foundation.

Data availability

All observational data, including the spectrophotometer data, are published in the Environmental Data Initiative repository (Carey et al., 2022a; Carey et al., 2022b; Carey et al., 2022c; Schreiber et al., 2022; Hammond et al., 2023). All code used to analyze the spectrophotometer data with PLSR and generate the figures is available in the Zenodo repository (Hammond 2022).

Acknowledgements

This work has been supported by the Virginia Tech Cunningham Doctoral Fellowship, the Geological Society of America Graduate Research Grant Program, and the National Science Foundation (DEB-1753639, CNS-1737424, DBI-1933016). We gratefully acknowledge the Western Virginia Water Authority for allowing us access to the reservoir to conduct these experiments and Jeff Parks for ICP-MS analysis. We also thank Abby Lewis, Heather Wander, and the entire Virginia Tech Reservoir Group research team for field support. We greatly appreciate the helpful feedback from four anonymous reviewers, which greatly improved the manuscript.

Supplementary materials

Supplementary material associated with this article can be found, in the online version, at doi:10.1016/j.watres.2023.120084.

References

Allen, E.L. 2021. Water Quality Signatures of Switchgrass (*Panicum Virgatum*) Intercropped in Managed Forests and Mixed Land Use in the Southeastern United States. *ProQuest Dissertations and Theses* (North Carolina State University).

Avagyan, A., Runkle, B.R.K., Kutzbach, L., 2014. Application of high-resolution spectral absorbance measurements to determine dissolved organic carbon concentration in remote areas. J. Hydrol. 517, 435–446. https://doi.org/10.1016/j.jhydrol.2014.05.060.

Beutel, M.W., Horne, A.J., 1999. A review of the effects of hypolimnetic oxygenation on lake and reservoir water quality. Lake Reserv. Manag. 15, 285–297. https://doi.org/10.1080/07438149909354124.

Birgand, F., Aveni-Deforge, K., Smith, B., Maxwell, B., Horstman, M., Gerling, A.B., Carey, C.C., 2016. First report of a novel multiplexer pumping system coupled to a water quality probe to collect high temporal frequency in situ water chemistry measurements at multiple sites. Limnol. Oceanogr. Methods 14, 767–783. https://doi.org/10.1002/lom3.10122.

Bryant, L.D., Hsu-Kim, H., Gantzer, P.A., Little, J.C., 2011. Solving the problem at the source: controlling Mn release at the sediment-water interface via hypolimnetic oxygenation. Water Res 45, 6381–6392. https://doi.org/10.1016/j.watres.2011.09.030.

Carey, C.C., A. Breef-Pilz, and B.J. Bookout. 2022a. Time series of high-frequency meteorological data at Falling Creek Reservoir, Virginia, USA 2015-2021 ver 6 [dataset]. Environmental Data Initiative. 10.6073/pasta/35d8d3f9390408f12d39e44e3f03abbe (Accessed 2022-09-30).

Carey, C.C., A. Breef-Pilz, W.M. Woelmer, and B.J. Bookout. 2022b. Time series of high-frequency sensor data measuring water temperature, dissolved oxygen, pressure, conductivity, specific conductance, total dissolved solids, chlorophyll a, phycocyanin, and fluorescent dissolved organic matter at discrete depths in Falling Creek Reservoir, Virginia, USA in 2018-2021 ver 6 [dataset]. Environmental Data Initiative. 10.6073/pasta/81c6c76f4fe22434a20aa8c00f2d4ad1 (Accessed 2022-02-02).

Carey, C.C., A.S. Lewis, D.W. Howard, W.M. Woelmer, P.A. Gantzer, K.A. Bierlein, J.C. Little, and WVWA. 2022c. Bathymetry and watershed area for Falling Creek Reservoir, Beaverdam Reservoir, and Carvins Cove Reservoir ver 1 [dataset]. Environmental Data Initiative. 10.6073/pasta/352735344150f7e77d2bc18b69a22412 (Accessed 2022-11-16).

Cao, D.S., Deng, Z.K., Zhu, M.F., Yao, Z.J., Dong, J., Zhao, R.G., 2017. Ensemble partial least squares regression for descriptor selection, outlier detection, applicability domain assessment, and ensemble modeling in QSAR/QSPR modeling. J. Chemom. 31, 1–17. https://doi.org/10.1002/cem.2922.

Chapman, M.J., Cravotta, C.A., Szabo, Z., Lindsey, B.D., 2013. Naturally Occurring Contaminants in the Piedmont and Blue Ridge Cystalline-rock Aquifers and Piedmont Early Mesozoic Basin Siliciclastic-rock Aquifers, Eastern United States, 1994-2008. US Department of the Interior, US Geological Survey.

Coraggio, E., Han, D., Gronow, C., Tryfonas, T., 2022. Water Quality Sampling Frequency Analysis of Surface Freshwater: a Case Study on Bristol Floating Harbour. Front. Sustain. Cities 3, 1–14. https://doi.org/10.3389/frsc.2021.791595.

Davison, W., Seed, G., 1983. The kinetics of the oxidation of ferrous iron in synthetic and natural waters. Geochim. Cosmochim. Acta 47, 67–79. https://doi.org/10.1016/0016-7037(83)90091-1.

Davison, W., 1993. Iron and manganese in lakes. Earth Sci. Rev. 34, 119–163. https://doi.org/10.1016/0012-8252(93)90029-7.

Denham, M.C., 1997. Prediction intervals in partial least squares. J. Chemom. 11, 39–52. 10.1002/(SICI)1099-128X(199701)11:1<39::AID-CEM433>3.0.CO;2-S.

Dent, S.R., Beutel, M.W., Gantzer, P., Moore, B.C., 2014. Response of methylmercury, total mercury, iron and manganese to oxygenation of an anoxic hypolimnion in North Twin lake. Washington. Lake Reserv. Manag. 30, 119–130. https://doi.org/10.1080/10402381.2014.898350.

Difoggio, R., 2000. Guidelines for applying chemometrics to spectra: feasibility and error propagation. Appl. Spectrosc. 54 https://doi.org/10.1366/0003702001949546.

Etheridge, J.R., Birgand, F., Osborne, J.A., Osburn, C.L., Burchell, M.R., Irving, J., 2014. Using in situ ultraviolet-visual spectroscopy to measure nitrogen, carbon, phosphorus, and suspended solids concentrations at a high frequency in a brackish tidal marsh. Limnol. Oceanogr. Methods 12, 10–22. https://doi.org/10.4319/lom.2014.12.10.

Gantzer, P.A., Bryant, L.D., Little, J.C., 2009. Controlling soluble iron and manganese in a water-supply reservoir using hypolimnetic oxygenation. Water Res. 43, 1285–1294. https://doi.org/10.1016/j.watres.2008.12.019.

Gerling, A.B., Browne, R.G., Gantzer, P.A., Mobley, M.H., Little, J.C., Carey, C.C., 2014. First report of the successful operation of a side stream supersaturation hypolimnetic oxygenation system in a eutrophic, shallow reservoir. Water Res. 67, 129–143. https://doi.org/10.1016/j.watres.2014.09.002.

Hammond, N.W., F. Birgand, C.C. Carey, A. Breef-Pilz, B. Bookout, and M.E. Schreiber. 2023. Time series of in situ ultraviolet-visible absorbance spectra and high-frequency predictions of total and soluble Fe and Mn concentrations measured at multiple depths in Falling Creek Reservoir (Vinton, VA, USA) in 2020 and 2021 ver 1 [dataset]. Environmental Data Initiative. 10.6073/pasta/9755e7d161fa2684d1575f07ecf5fd79.

Hammond, N.W. 2022. High-frequency sensor data capture short-term variability in Fe and Mn cycling due to hypolimnetic oxygenation and seasonal dynamics in a drinking water reservoir [code]. 10.5281/zenodo.7339718.

Hem, J.D., 1972. Chemical factors that influence the availability of iron and manganese in aqueous systems. Geol. Soc. Am. Bull. 83, 443–450.

Idso, S.B., 1973. On the concept of Lake Stability. Limnol. Oceanogr. 18, 681–683.

Istvánovics, V., Osztoics, A., Honti, M., 2004. Dynamics and ecological significance of daily internal load of phosphorus in shallow Lake Balaton. Hungary. Freshw. Biol. 49, 232–252. https://doi.org/10.1111/j.1365-2427.2004.01180.x.

Kankaala, P., Taipale, S., Nykänen, H., Jones, R.I., 2007. Oxidation, efflux, and isotopic fractionation of methane during autumnal turnover in a polyhumic, boreal lake. J. Geophys. Res. Biogeosciences 112, 1–7. https://doi.org/10.1029/2006JG000336.

Kritzberg, E.S., Hasselquist, E.M., Škerlep, M., Löfgren, S., Olsson, O., Stadmark, J., Valinia, S., Hansson, L.A., Laudon, H., 2020. Browning of freshwaters: consequences to ecosystem services, underlying drivers, and potential mitigation measures. Ambio 49, 375–390. https://doi.org/10.1007/s13280-019-01227-5.

Krueger, K.M., Vavrus, C.E., Lofton, M.E., McClure, R.P., Gantzer, P., Carey, C.C., Schreiber, M.E., 2020. Iron and manganese fluxes across the sediment-water interface in a drinking water reservoir. Water Res. 182, 116003 https://doi.org/10.1016/j.watres.2020.116003.

Kruse, P., 2018. Review on water quality sensors. J. Phys. D. Appl. Phys. 51 https://doi.org/10.1088/1361-6463/aabb93.

Kurz, M.J., de Montety, V., Martin, J.B., Cohen, M.J., Foster, C.R., 2013. Controls on diel metal cycles in a biologically productive carbonate-dominated river. Chem. Geol. 358, 61–74. https://doi.org/10.1016/j.chemgeo.2013.08.042.

Marcé, R., George, G., Buscarinu, P., Deidda, M., Dunalska, J., De Eyto, E., Flaim, G., Grossart, H.P., Istvanovics, V., Lenhardt, M., Moreno-Ostos, E., Obrador, B., Ostrovsky, I., Pierson, D.C., Potužák, J., Poikane, S., Rinke, K., Rodríguez-Mozaz, S., Staehr, P.A., Šumberová, K., Waajen, G., Weyhenmeyer, G.A., Weathers, K.C., Zion, M., Ibelings, B.W., Jennings, E., 2016. Automatic high frequency monitoring for improved lake and reservoir management. Environ. Sci. Technol. 50, 10780–10794. https://doi.org/10.1021/acs.est.6b01604.

McClain, M.E., Boyer, E.W., Dent, C.L., Gergel, S.E., Grimm, N.B., Groffman, P.M., Hart, S.C., Harvey, J.W., Johnston, C.A., Mayorga, E., McDowell, W.H., Pinay, G., 2003. Biogeochemical hot spots and hot moments at the interface of terrestrial and aquatic ecosystems. Ecosystems 6, 301–312. https://doi.org/10.1007/s10021-003-0161-9.

McClure, R.P., Hamre, K.D., Niederlehner, B.R., Munger, Z.W., Chen, S., Lofton, M.E., Schreiber, M.E., Carey, C.C., 2018. Metalimnetic oxygen minima alter the vertical profiles of carbon dioxide and methane in a managed freshwater reservoir. Sci. Total Environ. 636, 610–620. https://doi.org/10.1016/j.scitotenv.2018.04.255.

McMahon, J.W., 1969. The Annual and Diurnal variation in the vertical distribution of acid-soluble ferrous and total iron in a small dimictic Lake. Limnol. Oceanogr. 14, 357–367. https://doi.org/10.4319/lo.1969.14.3.0357.

Mevik, B.H., Wehrens, R., and Liland, K.H. (2020). pls: partial Least Squares and Principal Component Regression. R package version 2.7-3. https://CRAN.R-project.org/package=pls.

Müller, B., Bryant, L.D., Matzinger, A., Wüest, A., 2012. Hypolimnetic Oxygen Depletion in Eutrophic Lakes. Environ. Sci. Technol. 46, 9964–9971. https://doi.org/10.1021/es301422r.

Munger, Z.W., Carey, C.C., Gerling, A.B., Hamre, K.D., Doubek, J.P., Klepatzki, S.D., McClure, R.P., Schreiber, M.E., 2016. Effectiveness of hypolimnetic oxygenation for preventing accumulation of Fe and Mn in a drinking water reservoir. Water Res. 106, 1–14. https://doi.org/10.1016/j.watres.2016.09.038.

Munger, Z.W., Carey, C.C., Gerling, A.B., Doubek, J.P., Hamre, K.D., McClure, R.P., Schreiber, M.E., 2019. Oxygenation and hydrologic controls on iron and manganese mass budgets in a drinking-water reservoir. Lake Reserv. Manag. 35, 277–291. https://doi.org/10.1080/10402381.2018.1545811.

Nimick, D.A., Gammons, C.H., Parker, S.R., 2011. Diel biogeochemical processes and their effect on the aqueous chemistry of streams: a review. Chem. Geol. 283, 3–17. https://doi.org/10.1016/j.chemgeo.2010.08.017.

Porter, J.H., Nagy, E., Kratz, T.K., Hanson, P., Collins, S.L., Arzberger, P., 2009. New eyes on the world: advanced sensors for ecology. Bioscience 59, 385–397. https://doi.org/10.1525/bio.2009.59.5.6.

Poulin, B.A., Ryan, J.N., Aiken, G.R., 2014. Effects of iron on optical properties of dissolved organic matter. Environ. Sci. Technol. 48, 10098–10106. https://doi.org/10.1021/es502670r.

Preece, E.P., Moore, B.C., Skinner, M.M., Child, A., Dent, S., 2019. A review of the biological and chemical effects of hypolimnetic oxygenation. Lake Reserv. Manag. 35, 229–246. https://doi.org/10.1080/10402381.2019.1580325.

R Core Team (2022). R: A language and Environment For Statistical computing. R Foundation For Statistical Computing, Vienna, Austria. URL https://www.R-project.org/.

Rode, M., Wade, A.J., Cohen, M.J., Hensley, R.T., Bowes, M.J., Kirchner, J.W., Arhonditsis, G.B., Jordan, P., Kronvang, B., Halliday, S.J., Skeffington, R.A., Rozemeijer, J.C., Aubert, A.H., Rinke, K., Jomaa, S., 2016. Sensors in the stream: the high-frequency wave of the present. Environ. Sci. Technol. 50, 10297–10307. https://doi.org/10.1021/acs.est.6b02155.

Sakamoto, C.M., Johnson, K.S., Coletti, L.J., 2009. Improved algorithm for the computation of nitrate concentrations in seawater using an in situ ultraviolet spectrophotometer. Limnol. Oceanogr. Methods 7, 132–143. https://doi.org/10.1002/lom3.10209.

Schreiber, M.E., Hammond, N.W., Krueger, K.M., Munger, Z.W., Ming, C.L., Breef-Pilz, A., Carey, C.C., 2022. Time series of total and soluble iron and manganese concentrations from Falling Creek Reservoir and Beaverdam Reservoir in southwestern Virginia, USA from 2014 through 2021 ver 6. Environmental Data Initiative [dataset]. doi:10.6073/pasta/7cdf3d7a234963b265f09b7d6d08f357.

USEPA. 2021. Secondary Drinking Water Standards: guidance for Nuisance Chemicals. Available at: https://www.epa.gov/sdwa/secondary-drinking-water-standards-guidance-nuisance-chemicals. (Accessed: 22nd February 2021).

Thomas, R.Q., Figueiredo, R.J., Daneshmand, V., Bookout, B.J., Puckett, L.K., Carey, C. C., 2020. A near-term iterative forecasting system successfully predicts reservoir hydrodynamics and partitions uncertainty in real time. Water Resour Res 56, e2019WR026138. https://doi.org/10.1029/2019WR026138.

Vaughan, M.C.H., Bowden, W.B., Shanley, J.B., Vermilyea, A., Wemple, B., Schroth, A. W., 2018. Using in situ UV–Visible spectrophotometer sensors to quantify riverine phosphorus partitioning and concentration at a high frequency. Limnol. Oceanogr. Methods 16, 840–855. https://doi.org/10.1002/lom3.10287.

Wasserman, G.A., Liu, X., Parvez, F., Ahsan, H., Levy, D., Factor-Litvak, P., Kline, J., van Geen, A., Slavkovich, V., Lolacono, N.J., Cheng, Z., Zheng, Y., Graziano, J.H., 2006. Water manganese exposure and children's intellectual function in Araihazar. Bangladesh. Environ. Health Perspect. 114, 124–129. https://doi.org/10.1289/ehp.8030.

Weishaar, J.L., Aiken, G.R., Bergamaschi, B.A., Fram, M.S., Fujii, R., Mopper, K., 2003. Evaluation of specific ultraviolet absorbance as an indicator of the chemical composition and reactivity of dissolved organic carbon. Environ. Sci. Technol. 37, 4702–4708. https://doi.org/10.1021/es030360x.

Winslow, L., Read, J., Woolway, R., Brentrup, J., Leach, T., Zwart, J., Albers, S., Collinge, D., 2019. rLakeAnalyzer: lake Physics Tools. R package version 1.11.4.1. https://CRAN.R-project.org/package=rLakeAnalyzer.

Wold, S., Sjöström, M., Eriksson, L., 2001. PLS-regression: a basic tool of chemometrics. Chemom. Intell. Lab. Syst. 58, 109–130. https://doi.org/10.1016/S0169-7439(01)00155-1.

Woodward, H.P., 1932. Geology and Mineral Resources of the Roanoke Area, Virginia, Virginia Geological Survey. Bulletin 34.

World Health Organization, 2017. Guidelines for Drinking - Water Quality. Fourth Edition Incorporating the First Addendum. 10 Acceptability aspects: taste, odour and appearance.

Xiao, N., Cao, D.S., Li, M.Z., and Xu, Q.S. (2019). enpls: ensemble Partial Least Squares Regression. R package version 6.1. https://CRAN.R-project.org/package=enpls.

Xiao, Y.H., Sara-Aho, T., Hartikainen, H., Vähätalo, A.V., 2013. Contribution of ferric iron to light absorption by chromophoric dissolved organic matter. Limnol. Oceanogr. 58, 653–662. https://doi.org/10.4319/lo.2013.58.2.0653.